Design of a Decoupled MRI-compatible Force Sensor using Fiber Bragg Grating Sensors for Robot-assisted Prostate Interventions

Reza Monfaredi*[a], Reza Seifabadi[b], Gabor Fichtinger[b], and Iulian Iordachita[a]
[a]Laboratory for Computational Sensing and Robotics (LCSR), Johns Hopkins University, Baltimore, MD, USA
[b]Laboratory for percutaneous interventions (Perk Lab), School of Computing, Queens University, Ontario, Canada

ABSTRACT

During prostate needle insertion, the gland rotates and displaces resulting in needle placement inaccuracy. To compensate for this error, we proposed master-slave needle steering under real-time MRI in a previous study. For MRI-compatibility and accurate motion control, the master (and the slave) robot uses piezo actuators. These actuators however, are non-backdrivable. To cope with this issue, force sensor is required. Force sensor is also required at the slave side to reflect the insertion force to clinician's hand through the master robot. Currently, there is no MRI-compatible force sensor commercially available. In order to generate a combination of linear and rotary motions for needle steering, this study is seeking to develop a MRI-compatible 2 Degrees of Freedom (DOF) force/torque sensor. Fiber Brag Grating (FBG) strain measuring sensors which are proven to be MRI-compatible are used. The active element is made of phosphor-bronze and other parts are made of brass. The force and torque measurements are designed to be entirely decoupled. The sensor measures -20 to 20 N axial force with 0.1 N resolution, and -200 to 200 Nmm axial torque with 1 Nmm resolution. Analytical and Finite Element (FE) analyses are performed to ensure the strains are within the measurable range of the FBG sensors. The sensor is designed to be compact (diameter =15 mm, height =20 mm) and easy to handle and install. The proposed sensor is fabricated and calibrated using a commercial force/torque sensor.

Keywords: MRI-compatible force sensor, 2DOF Decoupled force/torque sensor, prostate intervention, MRI-guided needle steering.

1. INTRODUCTION

In the last decade, robot assisted MRI-guided prostate needle placement has gained a lot of interest due to the MRI superior imaging capabilities. MRI-compatible force/torque sensor could be an important part of robotic systems for prostate percutaneous interventions under MRI. Despite the advance reported recently in MRI-compatible systems, developing a proper MRI-compatible sensor is still a challenging task. To the best of our knowledge, there is no commercially available MRI-compatible sensor in the market and recent research in this field does not provide an applicable solution.

The application (Figure 1) for which we are developing a force sensor is teleoperated needle steering under real-time MRI guidance proposed in [1]. The clinician interacts with a master robot which is placed next to the scanner and therefore must be MRI-compatible. The slave robot which is installed on the base robot [2], [3] (the base robot orients the needle toward the target), follows the motions of the master.

*reza.monfaredi@jhu.edu; phone: 1-410-516-3839; amiro.lcsr.jhu.edu

Slave and master have 2 DOF each, linear motion for the needle plus the rotation of it. Since the needle is beveled, the combination of these two motions enables needle steering. Visual feedback is provided by real-time MRI. A controller is developed to enable communication between master and slave. The idea of teleoperation is proposed to enable the surgeon to remotely perform the task while the patient is inside the scanner for real-time imaging.

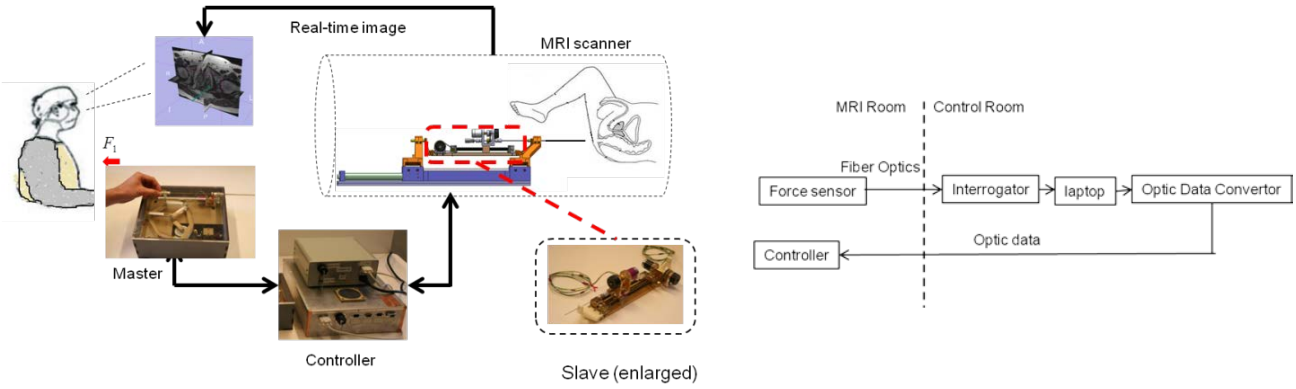

(a) (b)

Figure 1. (a) Teleoperated needle steering under real-time MRI-guidance is proposed to compensate for needle placement error; (b) the electronic parts for force measurement are placed outside the MRI room thus eliminating interference with magnetic field.

Since the master robot uses piezo motors for the sake of MRI-compatibility and ease of control, it is non-backdrivable. Therefore, a 2 DOF force-torque sensor is required to enable movement. In addition, to feedback the needle insertion force to the clinician's hand, a force sensor should be placed at the slave side behind the needle. Both force sensors should be MRI-compatible. MRI-compatibility for sensors means that: 1) the sensor should be able to operate in a high magnetic field and 2) it has minimal disturbance to the MRI images. This means that usage of any ferromagnetic parts should be reduced at minimum, and non-magnetic metallic parts should be avoided. In addition, it implies that the conventional strain gauges should be avoided since they distort the magnetic field and the RF pulse emitted by the scanner thus drastically degrading the image quality. Shielding of strain gauges does not resolve the image degradation.

In previous studies, hydrostatic pressure, differential light intensity, differential optic fiber, optical micrometry, and absolute light intensity have been proposed as alternatives to the conventional strain gauges [4]. Tada *et al.* [5] developed an optical 2-axis force sensor without any metal and electronic components in the sensing element using photo sensors and optical fibers. The sensor was a 2DOF sensor which measures forces in x and y directions and it was rather bulky since it used photo sensors.

Chapuis *et al.* [6] designed a simple and efficient torque sensor based on light intensity measurement over optical fibers. This sensor allowed the electronic components to be placed outside the scanner room. The sensitivity of transverse torque was reduced to 0.03% of the desired output torque by using a self-guiding flexible structure and optimal mirror placement. This sensor was a single DOF sensor for torque sensing and utilized optical technology for the compactness and being sensitive to precise placement of the mirrors.

A MRI-compatible three-axis force sensor was developed in [7]. Differential measure of light intensity is used to develop this sensor using a new MRI-compatible optical micrometry. Optoelectronic devices and pairs of fiber optics are used to measure forces in three directions. Two micrometers were aligned in orthogonal directions in order to realize three-axis force sensitivity.

Parallel plate structure was used to develop a MRI-compatible optical force sensor. It utilized an optical micrometry based on differential measures of light intensity [8]. The sensor's head component was made of glass fiber reinforced poly-ether-ether-ketone to reduce axial interference and hysteresis behavior of plastic resin. This was a 1DOF sensor for axial force sensing.

An optical fiber sensing method was designed and fabricated in [9]. The sensor was based on an optical sensing principle and measured forces by deforming a 3 DOF flexible structure. By using an optical sensing scheme minute

deflection of the structure was detected and then the magnitude and direction of the applied force was determined. This sensor measured only forces, and it was bulky because of the sensing principal.

Polygerinos *et al*. in [10] presented a prototype design and development of a small MRI-compatible fiber optic force sensor for force sensing during MRI-guided cardiac catheterization. A fiber optic cable interrogated a reflective surface at a predefined distance inside a catheter shaft based on light intensity modulation.

Tan *et al*. have developed a 3DOF axial force sensor with small coupling effects between DOFs. Using materials with hysteretic behavior, it was necessary to use Prandtl–Ishlinskii theory to address this behavior. The sensor was very bulky [11].

Hao Su *et al*. [4] developed a sensor for two DOF torque measurement and one DOF force measurement. This sensor is based on fiber optic and spherical mirror technology. The sensor was bulky and was not able to measure axial torque which is necessary for needle steering in prostate intervention.

Iordachita *et al*. designed and analyzed a force measurement device that measures distal forces interior to the sclera using FBGs embedded in a 0.5 mm diameter tool shaft. Utilizing FGB technology in this design made the device as small as possible which was necessary for retinal microsurgery. This device is proper for force sensing in 2 directions especially for microsurgery procedures [12].

As the literature review illustrates, there is a lack of a proper and compact 2DOF sensor for force/torque sensing which is required for prostate intervention by a master-slave system. In this study, we propose using FBG sensors as the strain measuring elements. FBG is a type of distributed Bragg grating constructed in a short segment of optical fiber that reflects a particular wavelength of light and transmits all others [13]. If FBG experiences strain which can be caused either by mechanical stress or thermal stress (i.e. external force/torque or temperature change), the distance between two consecutive layers changes, resulting in the shift of the reflected wavelength. This wavelength shift is a linear function of both the mechanical and thermal strain. Previously, FBG was used for needle shape tracking [14] and force measurement applied to the needle tip in retinal surgery [12]. However, no force/torque sensor with FBG has been reported yet. The advantages of FBG sensors are as follows: 1) they can measure a very high strain up to 5000 (even 10000) μm/m and therefore, they can offer a higher sensitivity; 2) they are bio-compatible; 3) they are sterilizable; 4) and they are easy to install.

Since the optic fibers are utilized not only for strain measurement, but also for data transformation, they do not interfere with the MRI machine's magnetic field in any way. The interrogator (which is the signal analyzer device and generates the light and computes the wavelength shift based on the reflected signal) is placed outside the MRI room, thus it has no impact on MRI image (Fig. 1 (b)). The calibration matrices are then applied to the wavelength shift reading on a laptop next to the interrogator in order to generate the force data. The controller software is installed on the same laptop. Force measurements are then input to the controller software to produce the control law which will be sent to the master and slave robots through the optical data convertor. This procedure ensures no interference of the force sensing with MRI since it requires no electric signal transmission.

In this paper we present a new fully decoupled 2DOF sensor using FBGs. In section 2, the design procedure is described. Section 3 demonstrates the fabrication stage and FBGs installation. Section 4 discusses the calibration setup and results, and section 5 concludes the paper.

2. SENSOR DESIGN

2.1 Mechanical design

The following criteria are considered while designing the mechanical structure of the sensor: 1) *Decoupled sensor*: This will simplify the calibration procedure for the sensor. This criterion is fulfilled by utilizing a ball bearing and square cross section shaft to separate axial force and axial torque flow. 2) *Small size sensor*: This is necessary for the placement of the sensor in the intervention device. This criterion is considered by compact mechanical design and utilizing of FBGs with 2mm active length as the sensing element. 3) *Limitations of FBG installation***:** There are a few limitations which should be considered while designing the sensor, *i.e. FBG curvature limitation*: The FBG is embedded in a fiber and should not be overbent and *Beam-to-FBG length ratio*: There are some specific FBGs with standard active lengths available in the market. In this design, FBGs with 2 mm active length are selected as sensing elements. There is no standard for beam to FBG length ratio, but due to the stress concentration on the two extremities of the beam in which

the FBG are installed and to avoid the effect of this inconsistency on the BFG performance, beam-to-FBG length ratio must be fairly larger than 1. In our design 2 was selected. The FBG active length and the beam-to-FBG length ratio directly affect the size of the sensor and determine how small the sensor could be. 4) *No hysteresis and no fatigue*: Hysteric behavior is one of the probable problems which could be encountered in the sensor development. This problem is caused by the material used for the active elements. Basically, some of the materials have hysteric behavior. On the other hand, it should be noted that the active element is exposed to dynamic loading and unloading that could result in fatigue and failure of the sensor. In our design, phosphor bronze was considered as the material for active elements due to its hysteresis-free characteristic and high strength against dynamic loading and fatigue. Beside these advantages of the phosphor bronze, this material shows a good machinability making the fabrication easy. 5) *Temperature compensation***:** FBGs are very sensitive to the temperature variation. To deal with this problem, a set of two FBGs are used for each DOF. Using two FBGs and considering differential calculation, the temperature variation effect has been completely compensated.

In this section, two different decoupled designs are proposed and compared (Fig. 2 and Fig. 3). Figure 2(a) and Figure 3(a) show the exploded view of the proposed designs and where the FBGs are installed. As shown in these figures, four FBGs are used for a 2DOF sensor. Two FBGs are used for each DOF to compensate for temperature changes. In these figures, parts 1 and 6 are the two ends of the sensor to connect the sensor to the test bed. Part 2 is a ball bearing and is used to decouple the force and torque making it possible to measure them independently. Part 3 exerts the axial force to the corresponding FBGs. Part 4 has a square hole in the center which transmits torque but not the axial load. In the first design (Fig. 2), FBGs for axial force measurement are installed on part 5 while FBGs measuring the torque are installed on part 4. In the second proposed structure (Fig. 3), both FBGs corresponding to axial force and torque are installed on part 5. Figure 2(b) shows the assembled sensor for the first design. Figure 3(b) shows how the force and torque are separated using ball bearing for the second design and figure 3(c) shows how the torque flows from part1 to part6.

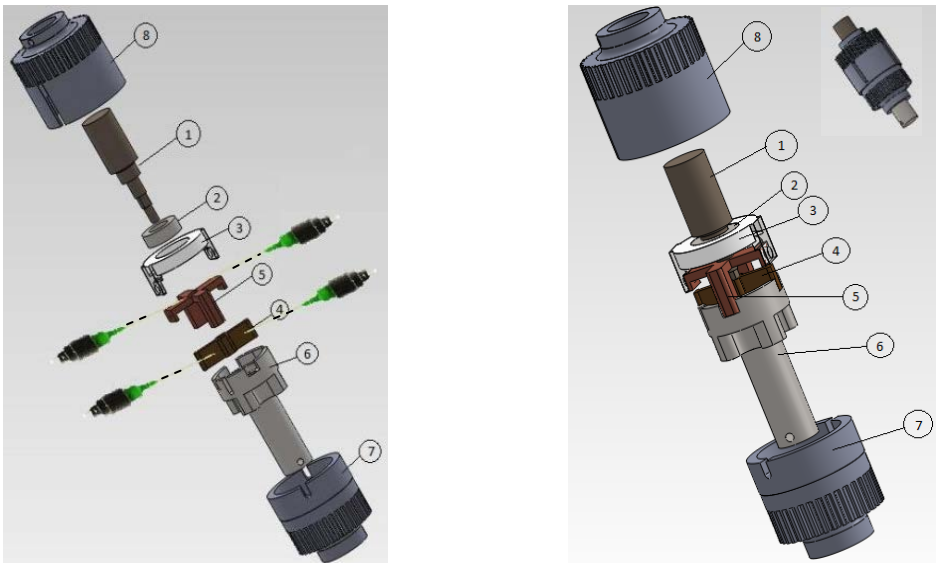

(a) (b)

Figure 2. 2DOF force/torque sensor with radial FBG installation, first design: (a) exploded view, (b) assembled sensor (1- square cross section shaft for torque transmitting; 2- ball bearing; 3- part for transmitting axial force; 4- active element for axial torque; 5- active element for axial force; 6- base and shaft; 7 and 8 are casings).

Mechanical decoupling of the sensor simplifies calibration of the sensor since the calibration matrix becomes diagonal in this case:

$$\begin{bmatrix}\Delta\lambda_1\\ \Delta\lambda_2\end{bmatrix} = \overbrace{\begin{bmatrix}c11 & 0\\ 0 & c22\end{bmatrix}}^{\mathbf{C}}\begin{bmatrix}f_z\\ \tau_z\end{bmatrix} \quad (1)$$

where C is the calibration matrix. Each element of this matrix could be found independently. f_z and τ_z are the axial force and torque, respectively. $\Delta\lambda_1$and $\Delta\lambda_2$ are the wavelength shifts of the force and torque active elements, respectively.

The functionality of both proposed designs are the same. However, in the second design (Fig. 3) the FBGs are installed axially rather than radially. Second design is advantageous to our application since it makes handling of the sensor easier and prevents the FBGs from damage. This is the preferred solution we built and calibrated.

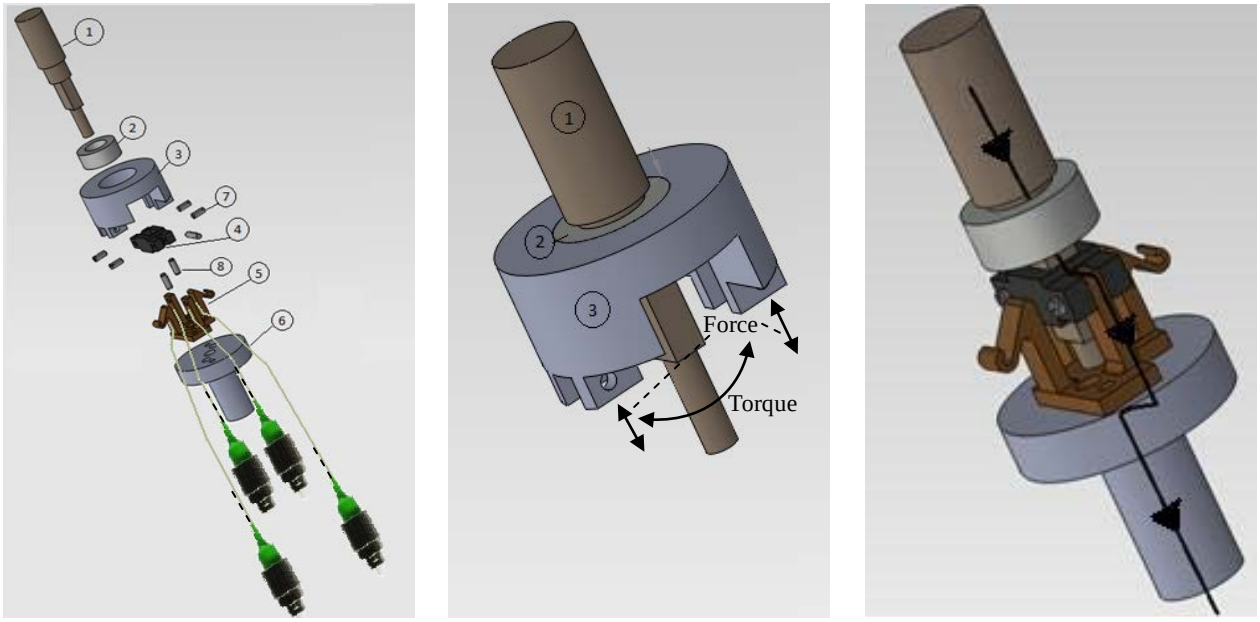

(a) (b) (c)

Figure 3. Modified sensor with axial FBG installation configuration: (a) exploded view, (b) ball bearing (part 2) connects part1 to part 3 with minimum friction thus decoupling force and torque measurement, and (c) the solid line shows how the torque flows from part1 to part6. (1- square cross section shaft for torque transmitting; 2- ball bearing; 3- part for transmitting axial force; 4- part for transmitting axial torque; 5- active element for axial force and torque; 6- base and shaft).

Part 5 (active element, Fig.3) is made of phosphor-bronze which is a MRI-compatible material and has hysteresis free behavior. The Elasticity module is $E = 1.1 \times 10^{11} N/m^2$. The force range of - 20 to +20N and torque range of -200 to 200 Nmm are considered as the working ranges of the sensor; the resolution is considered to be 0.1 N and 1 Nmm, respectively. The strain range of 5 to 1000 μϵ is selected for the FBG sensor. Considering the desired forces and strains, the thickness and the lengths of the beams could be designed using the following equation:

$$\epsilon = \frac{3FL}{2Et^2w} \quad (2)$$

Where *F* is the force applied to the end of the beam, *L* is the length of the beam, *E* is the Elasticity module, *t* and *w* are the thickness and width of the beam, respectively. According to equation (2), the following values yield: *L*= 4mm, *t* = 1 mm and *w* = 2 mm. Fig. 4(a) shows these parameters on the active element.

2.2 Finite element analysis

The FE analysis is used to investigate the strengths as well as linear behavior of the part on which the FBGs are installed (i.e. active elements). Figure 4(b) illustrates FE results for part 5 when axial force is exerted on the sensor (Fig. 3). Figure 4(a) shows the location for installing FBGs for axial load. The results show that actual stress is below the yield stress (Fig. 4(b)). Since axial force causes bending of the active elements (the beams on which FBGs are installed), it is important to keep the arm d in figure 4(b) constant and to prevent the lateral displacement of the applied force which will

cause inaccuracy is force measurement. Therefore, the beams were designed to have that specific shape as shown in figure 4(b). Simulation results confirm negligible lateral displacement.

Figure 5(a) shows why parts 4 and 5 were designed not to be a single piece. As seen, because of torsion the gradient of stress varies in lateral direction as well as longitudinal direction, which is not proper for the beam that FBGs will be installed on. The stress distribution along the beam is shown in figure 5(b) when part 4 and part 5 are connected using four set screws to apply concentrated force in contact points (Fig. 5(c)).

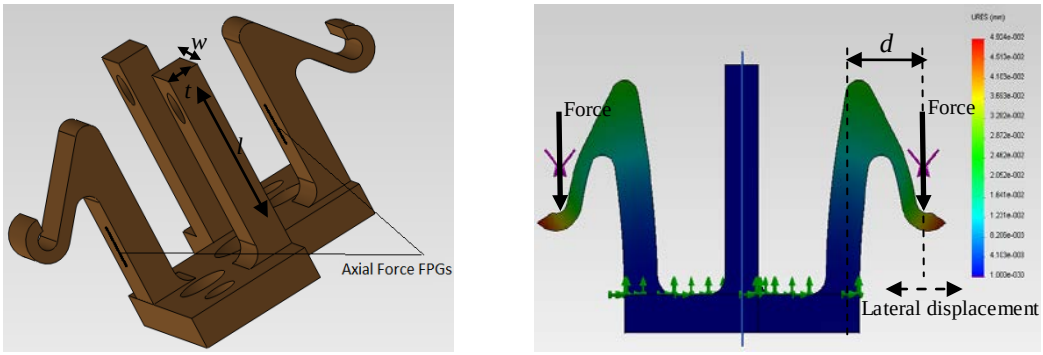

(a) (b)

Figure 4. (a) Active element, (b) FE results for axial force deformation (simulation shows that the tips of the L-shaped beams do not move in lateral direction, *i.e.* the arm d remains constant after applying the force).

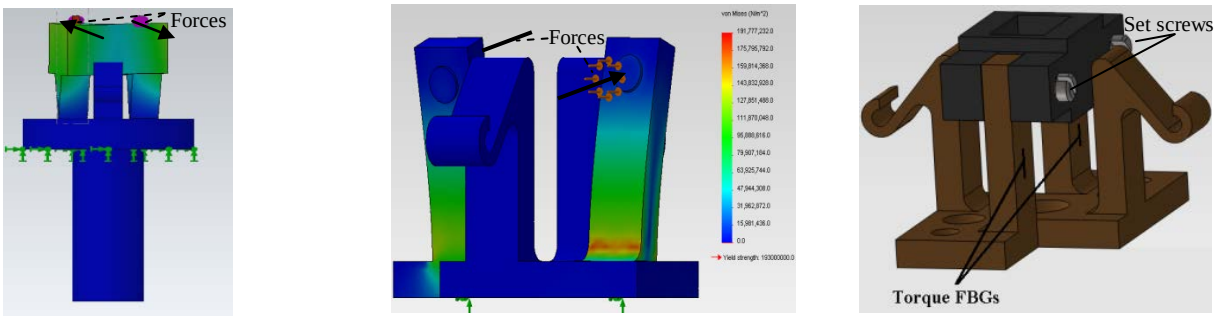

(a) (b) (c)

Figure 5. (a) Stress distribution when a single part is used for torque transfer, (b) stress distribution when two separate parts are used for torque transfer, and (c) close-up view of parts 4 and 5.

3. SENSOR FABRICATION AND FBG INSTALLATION

Since our sensor is not a rigid structure and a simple calibration procedure is sought for sensor calibration due to the decoupled structure of the sensor, the dimensional and geometrical tolerances of the parts after fabrication could affect the performance of the sensor. Therefore, a precise fabrication technology should be used specially for the active element. The active element (Fig. 4(a)) is manufactured by Wire EDM machine after redesigning of the part and dividing the active part to five different pieces.

Figure 6 illustrates five different pieces of the active element which were cut by Wire EDM machine and then were attached using high strength (2600 psi) plastic steel epoxy (ITW Devcon, Danvers, MA) to make an integrated part. Figure 7 shows an exploded view of the final parts. For the active element, phosphor bronze was used. Other metallic parts were made of brass. The casings were made of ABS material using rapid prototyping U print machine.

The ball bearing is a ceramic ball bearing which is nonmetallic and MRI-compatible. Figure 8 demonstratesthe fabricated and assembled sensor. Figure 8 shows that the size of our sensor is small. Figure 9 shows the final sensor with four FBGs which is ready to be plugged into the interrogator for calibration.

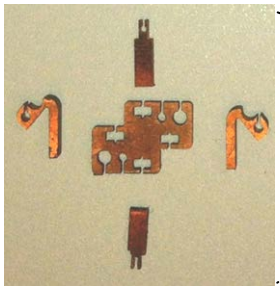

Figure 6. Different pieces of the active element which are fabricated by Wire EDM and are glued to each other.

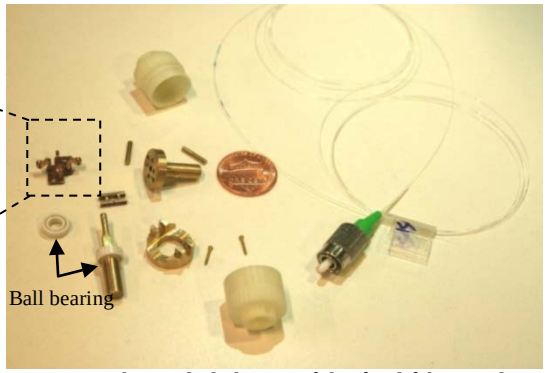

Figure 7. The exploded view of the final fabricated parts (See fig. 3(a) for labels of the parts).

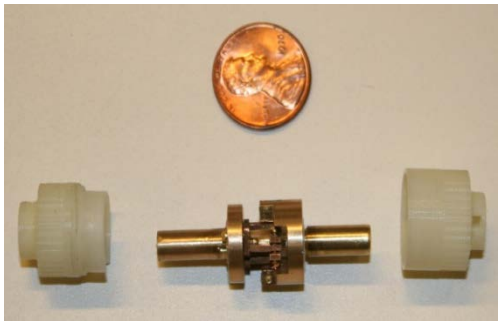

Figure 8. Assembled sensor (without FBG).

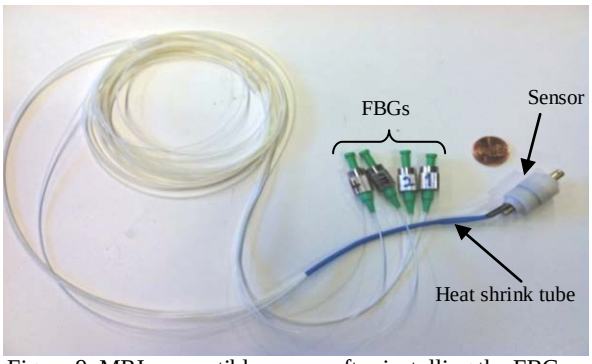

Figure 9. MRI-compatible sensor after installing the FBG.

The proper design of the sensor and placement of the FBGs have simplified the handling of the sensor since fibers are well secured using heat shrink tubes (Fig. 9).

4. SENSOR CALIBRATION AND RESULTS

Our sensor is fully and structurally decoupled and as a result it is very easy to be calibrated compared to other sensors. A small size lathe (Model 4410, Sherline Products, Inc., Vista, CA) was used to calibrate the sensor. We needed two DOFs for our calibration setup, one axial motion and one axial rotation to apply axial force and torque to the sensor. As shown in fig. 10(a), a commercial 6DOF Nano17 sensor (ATI Industrial Automation, Apex, NC) was used for calibration. Nano17 sensor and our MRI-compatible sensor were attached in series by using a flexible coupling. This set of sensors is fixed to the lathe machine between lathe jaw chuck and tailstock chuck as an integrated part. Then, it was possible to apply torque to the sensors by applying torque to the jaw chuck and to apply axial force by moving the tailstock chuck in lathe's axial direction by rotating the handwheel.

Figure 10(b) shows the complete setup for our sensor calibration procedure. FBGs are connected to the interrogator (sm 130, Micron Optics, Inc., Atlanta, GA) and the interrogator is connected to the laptop/Matlab via network connection port and UDP protocol. The Nano 17 sensor was connected to the laptop/Matlab via a Galil controller DAQ (DB 28040, Galil Motion Control, Rocklin, CA). The outputs of both, the Nano 17 sensor and MRI-compatible sensor, were processed in Matlab software to estimate the calibration matrix.

For calibration of the axial force, we used the handwheel to move the tailstock chuck and to increase the axial force gradually. The output of the Nano 17 sensor was plotted versus $\Delta\lambda_1$. The slope of the obtained calibration line was considered as the calibration coefficient, i.e. FMRI Sensor$= C_1.\Delta\lambda_1$, where C_1 is the above mentioned coefficient. The same procedure was conducted for the calibration of the axial torque.

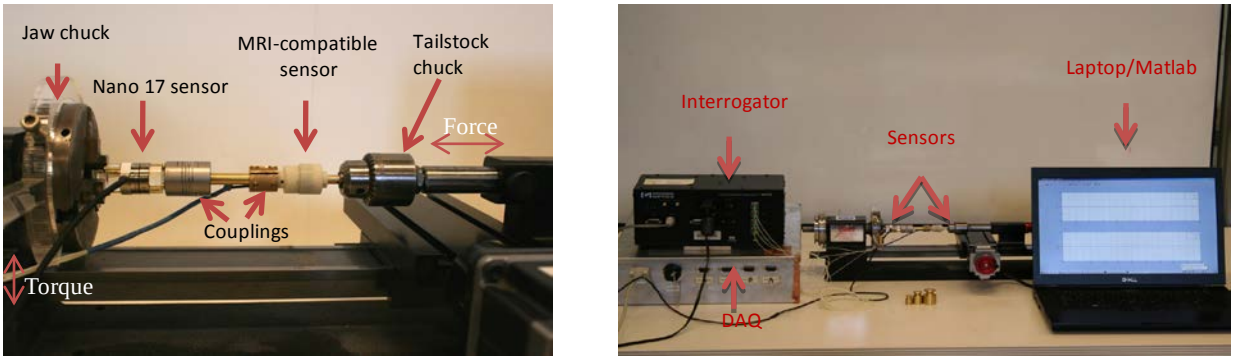

(a) (b)

Figure 10. Calibration setup: a) close-up view of sensors; b) overall view.

For this case, a range of standard weights were used to apply torque on the jaw chuck by an extended arm. The axial force and torque were applied in both directions. Figures 11(a) and 11(b) show the calibration results for the axial force and axial torque, respectively.

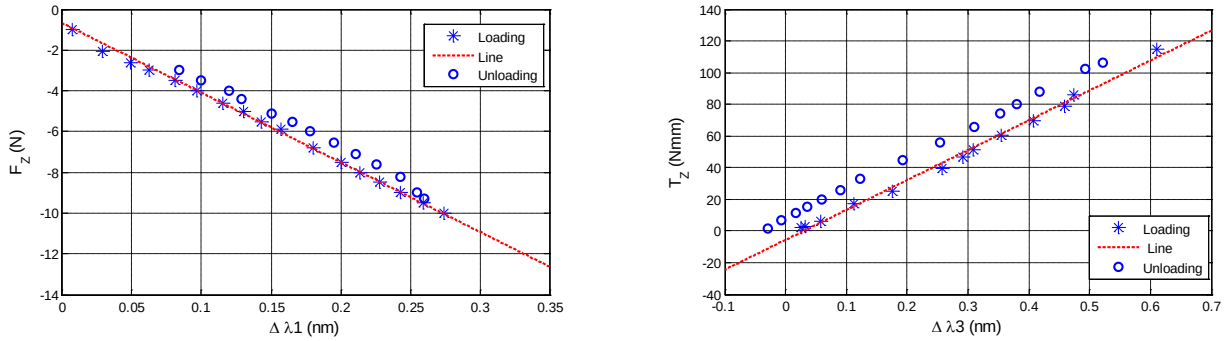

(a) (b)

Figure 11. Sensor calibration results: (a) axial force; (b) axial torque.

Results (Fig.11) show linear behavior of the sensor for axial force and axial torque loading and unloading. In these figures, there are some shifts between loading and unloading both in axial force and axial torque. These shifts are caused because of several reasons: 1) installation of the FBGs on two beams instead of four beams that caused asymmetric structure and made the sensor sensitive to lateral force and force distribution, 2) manufacturing errors especially an undesired clearance between part 1 and 6 (Fig. 3) which caused undesired sensitivity of the sensor to lateral forces, and 3) the assembling inaccuracy of the sensors in the calibration setup which could cause lateral forces.

5. CONCLUSIONS

A structurally inherent decoupled MRI force/torque sensor was designed, fabricated and calibrated to be used in a master-slave needle steering procedure under real-time MRI utilizing Fiber Bragg Grating technology. Structurally decoupled sensor prevents interference of force and torque in different directions, thus it was easier to be calibrated and provides better accuracy. Sensor design requirements were analyzed and two designs were proposed and compared. Finally FE analysis was performed and analyzed to finalize the configuration and dimensions of the preferred design sensor's elements. The proposed sensor was fabricated and calibrated using a commercial force/torque sensor. The calibration results show linear behavior of the sensor, but it also demonstrates a shift in the diagram in loading and unloading which was due to manufacturing errors and calibration setup and will be addressed in the future.

REFERENCES

[1] Seifabadi, R., Iordachita, I., and Fichtinger, G., “Design of a teleoperated needle steering system for MRI-guided prostate interventions”. 4th IEEE RAS & EMBS International Conference on Biomedical Robotics and Biomechatronics (BioRob), 793-798 (2012)

[2] Seifabadi, R., Cho, N. B., Song, S. E., Tokuda, J., Hata, N., Tempany, C. M.,and Iordachita, I. "Accuracy study of a robotic system for MRI-guided prostate needle placement", International Journal of Medical Robotics and Computer Assisted Surgery, 7(2), 181-190,(2012).

[3] Tokuda, J., Song, S. E., Fischer, G. S., Iordachita, I. I., Seifabadi, R., Cho, N. B., and Hata, N., "Preclinical evaluation of an MRI-compatible pneumatic robot for angulated needle placement in transperineal prostate interventions," Int JCARS, 7(6), 949-957, (2012).

[4] Su, H., and Fischer, G. S., "A 3-Axis Optical Force/Torque Sensor for Prostate Needle Placement in Magnetic Resonance Imaging Environments," IEEE International Conference on Technologies for Practical Robot Applications, 5-9 (2009).

[5] Tada, M., Sasaki, S., and Ogasawara, T., "Development of an optical 2-axis force sensor usable in MRI environments," Proc. of the IEEE Sensors, 2, 984 - 989 (2002).

[6] Chapuis, D., Gassert, R., Sache, L., Burdet, E., and Bleuler, H., "Design of a Simple MRI/fMRI Compatible Force/Torque Sensor," Proceedings of 2004 IEEE/RSJ International Conference on Intelligent Robots and Systems, 3, 2593-2599(2004).

[7] Tada, M., and Kanade, T., "Design of an MR-compatible three-axis force sensor," IEEE/RSJ International Conference on Intelligent Robots and Systems, 3505-3510 (2005).

[8] Tokuno, T., Tada, M., and Umeda, K., "High-Precision MRI-Compatible Force Sensor with Parallel Plate Structure," Proceedings of the 2nd Biennial IEEE/RAS-EMBS International Conference on Biomedical Robotics and Biomechatronics, 33-38 (2008).

[9] Puangmali, P., Althoefer, K., and Seneviratne, L. D., "Novel Design of a 3-Axis Optical Fiber Force Sensor for Applications in Magnetic Resonance Environments," IEEE International Conference on Robotics and Automation, 3682-3687 (2009).

[10] Polygerinos, P., Puangmali, P., Schaeffter, T., Razavi, R., Seneviratne, L. D., and Althoefer, K., "Novel Miniature MRI-Compatible Fiber-Optic Force Sensor for Cardiac Catheterization Procedures," IEEE International Conference on Robotics and Automation, 2598-2603 (2010).

[11] Tan, U., Yang, B., Gullapalli, R., and Desai, J. P., "Triaxial MRI-Compatible Fiber-optic Force Sensor," IEEE Transactions on Robotics,27(1), 65-74 (2011).

[12] Iordachita, I., Sun, Z., Balicki, M., Kang. J. U., Phee, S. J., Handa, J., Gehlbach., P., and Taylor, R., "A sub-millimetric, 0.25 mN resolution fully integrated fiber-optic force-sensing tool for retinal microsurgery," Int J CARS, 4(4), 383-390 (2009).

[13] Hill, K. O., and Meltz, G., "Fiber Bragg grating technology fundamentals and overview," Journal of Lightwave Technology, 15(8),1263–1276 (1997).

[14] Yong-Lae, P., Elayaperumal, S., Daniel, B., Ryu, S. C., Shin, M., Savall, J., Black R. J., Moslehi, B., and Cutkosky, M. R. "Real-Time Estimation of Three-Dimensional Needle Shape and Deflection for MRI-Guided Interventions," IEEE/ASME Trans. Mechatronics-Focused Section on Surgical and Interventional Medical Devices, 15(6), 906-915 (2010).